On the depletion of gadolinium-bearing fuel rods in BWR assemblies: a study within the NEA/OECD benchmark

Problematyka wypalania prętów paliwowych z gadolinem w zestawach reaktora wodnego wrzącego – benchmark NEA OECD

Łukasz Koszuk
Faculty of Physics, Warsaw University of Technology

Abstract: This paper presents the results obtained by the author within the framework of the OECD/NEA international benchmark: "Code comparison for depletion of gadolinium-bearing fuel rods in Boiling Water Reactor assemblies", dedicated to the validation of computer codes for modelling the burnup of Boiling Water Reactor (BWR) fuel containing gadolinium as a burnable absorber. The main objective of the benchmark was to analyze the capability of various computational systems to accurately predict the evolution of reactivity, with a particular focus on the „reactivity peak" phenomenon, which is crucial for criticality safety analyses and the burnup credit concept. The calculations were performed using the SCALE 6.2.2 code package (TRITON/NEWT sequence) with the 252-group ENDF/B-VII.1 nuclear data library. The paper presents the evolution of the k-inf multiplication factor, changes in the concentrations of key gadolinium isotopes (Gd-155, Gd-157), and detailed isotopic compositions of actinides and fission products for various burnup depths and three different water void fractions (0%, 40%, 70%). The obtained results showed very good agreement with the results of other benchmark participants, correctly reproducing both the general trends and numerical values. The summary also refers to the general conclusions from the OECD report, identifying nuclear data libraries as the main source of discrepancies in the results and highlighting the remaining challenges in modeling the concentrations of certain isotopes.

Keywords: BWR reactor, gadolinium, burnable absorber, fuel burnup, criticality safety, burnup credit, OECD/NEA benchmark, SCALE code.

Streszczenie: *Artykuł prezentuje wyniki uzyskane przez autora w ramach międzynarodowego benchmarku OECD/NEA pt. „Porównanie kodów obliczeniowych dla wypalania prętów paliwowych z gadolinem w zestawach reaktora wodnego wrzącego", poświęconego walidacji kodów obliczeniowych do modelowania wypalenia paliwa reaktora wodnego wrzącego (BWR) zawierającego gadolin jako wypalającą się truciznę. Głównym celem benchmarku była analiza zdolności różnych systemów obliczeniowych do precyzyjnego przewidywania ewolucji reaktywności, ze szczególnym uwzględnieniem tzw. piku reaktywności, który jest kluczowy dla analiz bezpieczeństwa krytycznościowego i koncepcji burnup credit. Obliczenia wykonano przy użyciu pakietu kodów SCALE 6.2.2 (sekwencja TRITON/NEWT) z wykorzystaniem 252-grupowej biblioteki danych jądrowych ENDF/B-VII.1. W pracy przedstawiono ewolucję współczynnika mnożenia k-inf, zmiany stężeń kluczowych izotopów gadolinu (Gd-155, Gd-157) oraz szczegółowe składy izotopowe aktynowców i produktów rozszczepienia dla różnych głębokości wypalenia i trzech wariantów zawartości pary w wodzie (0%, 40%, 70%). Uzyskane wyniki wykazały bardzo dobrą zgodność z rezultatami innych uczestników benchmarku, poprawnie odwzorowując zarówno ogólne trendy, jak i wartości liczbowe. W podsumowaniu odniesiono się także do ogólnych wniosków z raportu OECD, wskazując na biblioteki danych jądrowych jako główne źródło rozbieżności w wynikach oraz na wciąż istniejące wyzwania w modelowaniu stężeń niektórych izotopów.*

Słowa kluczowe: *Reaktor BWR, gadolin, wypalająca się trucizna, wypalanie paliwa bezpieczeństwo krytycznościowe, burnup credit, benchmark OECD/NEA, kod SCALE.*

1. Introduction

Modern fuel assemblies used in boiling water reactors (BWRs) often employ gadolinium oxide (Gd_2O_3) as a burnable neutron absorber (so-called burnable poison). Its presence leads to a complex reactivity behaviour of the fuel during operation. The rapid depletion of the strongly absorbing gadolinium isotopes causes the reactivity of the fuel assembly to initially increase, reaching a maximum at relatively low burnup (typically below 20 GWd/MTU), and then to decrease steadily. Accurate prediction of the characteristics of this reactivity peak is a fundamental challenge in criticality safety analyses, particularly in the context of implementing the *burnup credit* (BUC) approach for spent fuel.

To validate and compare the capabilities of computational systems in modelling such complex phenomena, the OECD Nuclear Energy Agency (NEA), through its Working Party on Nuclear Criticality Safety (WPNCS), organises international code comparison exercises (benchmarks). The direct motivation for organising Phase IIB of the benchmark – Code Comparison for Depletion of Gadolinium-Bearing Fuel Rods in Boiling Water Reactor Assemblies [1] – came from the results of the earlier Phase IIIC, which revealed significant discrepancies arising from differences in the modelling options chosen by the participants. In response, the Expert Group on Used Nuclear Fuel Criticality (EGUNF) designed Phase IIB with the key objective of isolating and assessing the differences resulting directly from the computational methods and nuclear data libraries used. To achieve this, the benchmark specification – based on the geometry of the 9 9 "STEP-3" fuel assembly – adopted a rigorous prescriptive approach. A unified, detailed gadolinium-bearing rod model (divided into 10 concentric rings) was imposed on all participants, along with precisely defined depletion steps, focusing the analysis on the reactivity peak region of critical safety significance.

The purpose of this paper is to present and analyse in detail the author's results for the Phase IIB benchmark. The work documents the application of a selected computational methodology to solving the complex issue of gadolinium-bearing BWR fuel depletion, in strict accordance with the OECD/NEA specification. The presented results and conclusions contribute to the documentation and understanding of the behaviour of such models, while the benchmark itself constitutes a valuable tool in the development of spent fuel safety analysis methods.

2. Burnable poisons

A burnable poison (or burnable absorber) is a material with a high neutron absorption cross section that is intentionally introduced into the core of a nuclear reactor. The primary purpose of using burnable poisons is to compensate for the excess reactivity of fresh fuel at the beginning of the reactor operating cycle. This allows for the safe loading of higher-enriched fuel, which in turn enables an extended fuel cycle length (the period of reactor operation between refuellings) and contributes to a more uniform power distribution within the core.

The operating mechanism of a burnable poison is that, during reactor operation, under neutron flux, the absorbing material is transmuted into isotopes with much smaller neutron absorption cross sections or into stable isotopes. In this way, the poison "burns out" and its negative contribution to reactivity decreases. This process causes a gradual increase in reactivity, partially offsetting the reactivity decrease resulting from the depletion of fissionable material and the accumulation of neutron-absorbing fission products. Figure 1 illustrates this effect by plotting the infinite multiplication factor of an example fuel assembly in two configurations — with and without a gadolinium-bearing rod — as a function of depletion time.

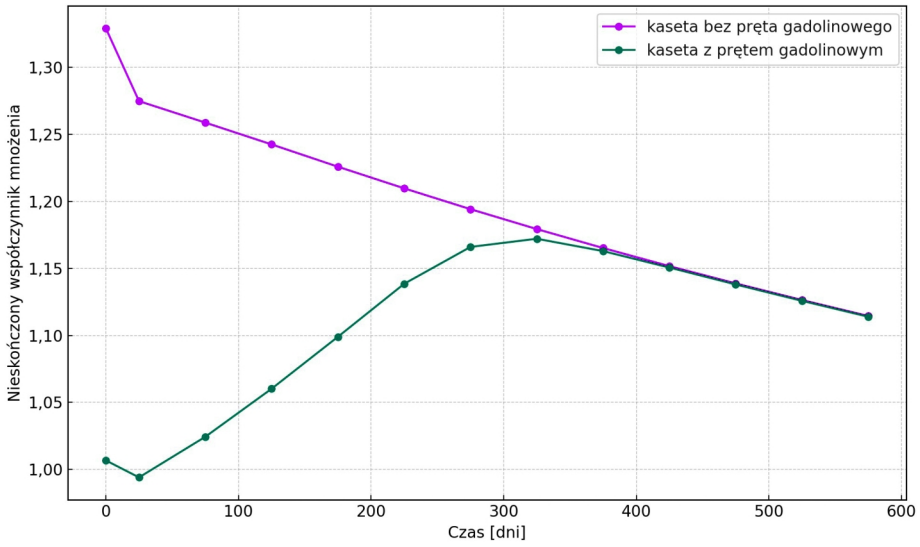

Fig. 1. Dependence of the infinite multiplication factor on the burnup time for the fuel assembly in two configurations: with and without a gadolinium rod. A characteristic reactivity peak is visible, caused by the presence of gadolinium in the nuclear fuel. Source: author's own work.

The most commonly used burnable absorber materials include gadolinium oxide (Gd_2O_3), erbium oxide (Er_2O_3), dysprosium compounds, and hafnium [2]. The choice of a particular material depends on the type of reactor, the fuel design and the desired depletion characteristics. In both pressurised water reactors (PWRs) and boiling water reactors (BWRs), the dominant and most widely used burnable absorber is gadolinium oxide, added to selected fuel rods.

3. Gadolinium oxide (Gd_2O_3)

The popularity of gadolinium oxide as a burnable absorber stems from the unique combination of its properties. A key feature of gadolinium is the exceptionally large thermal neutron absorption cross sections of its two naturally occurring isotopes: Gd-155 and Gd-157 The thermal (n,) capture cross section (for neutrons at 0.0253 eV) is approximately 254.000 barns for Gd-157 and about 61.100 barns for Gd-155 [3]. These values are several orders of magnitude higher than those for fissionable materials (e.g., ~580 barns for U-235) or even for other strong reactor poisons. This property means that even small amounts of gadolinium can effectively reduce the local neutron flux and control reactivity.

The isotopic composition of natural gadolinium is significant from the point of view of absorption efficiency: even-mass isotopes with smaller cross-sections differ (Gd-158 approx. 24.84%, Gd-160 approx. 21.86%, Gd-156 approx. 20.47%), while the main absorbers are Gd-155 (approx. 14.80%) and Gd-157 (approx. 15.65%) (others: Gd-154 approx. 2.18%, Gd-152 approx. 0.20%) [6]. Thus, ~30% of natural gadolinium constitutes isotopes with very large cross-sections, which correspond to the rapid "burnout" of the gadolinium additive.

In addition to its nuclear properties, Gd_2O_3 has a number of physicochemical advantages:

- At elevated temperatures, Gd_2O_3 dissolves well in uranium dioxide, allowing for homogeneous mixing with nuclear fuel during manufacturing to produce so-called UO_2–Gd_2O_3 fuel [4].
- Gadolinium oxide has a high melting point (approx. 2.420°C) and exhibits excellent chemical and radiation stability under reactor operating conditions. Importantly, upon neutron absorption it does not generate significant amounts of gaseous transmutation products [5]. This contrasts with boron, for example, whose B-10 isotope produces helium via the (n,á) reaction, potentially leading to increased rod internal pressure and fuel swelling.

Nevertheless, the use of gadolinium also has certain drawbacks. Once the main absorbers (Gd-155 and Gd-157) have been depleted, the remaining isotopes—especially the even-mass ones such as Gd-154, Gd-156, Gd-158, and Gd-160—have much smaller absorption cross sections and remain in the fuel as so-called *residual poison*. This can adversely affect neutron economy toward the end of the fuel cycle, reducing the achievable depletion. [4]

3.1 Challenges in modelling the depletion of gadolinium bearing fuel

Simulating the depletion of nuclear fuel is a complex task requiring the simultaneous solution of the neutron transport equation and the system of differential equations describing the evolution of the isotopic composition of the fuel over time. The presence of gadolinium, due to its unique properties, increases this complexity and introduces a range of challenges that must be accurately addressed in computational codes. Although the following challenges are discussed in the context of gadolinium, many of them are of a general nature and apply to modelling any material with very strong neutron-absorbing properties.

The following key issues can be identified when modelling the depletion of fuel containing a strong neutron absorber, particularly gadolinium.

a) Very large neutron absorption cross sections of Gd-155 and Gd-157 isotopes

The extremely high thermal neutron capture cross sections of gadolinium's two natural isotopes, Gd-155 and Gd-157 (values given in Section 3), are one of the main difficulties in modelling gadolinium-bearing fuel. To accurately track the rapid changes in gadolinium isotope concentrations and the resulting reactivity variations (especially near the reactivity peak), depletion calculations must be performed using small time steps (or, equivalently, small depletion steps).

b) Strong self-shielding effects

A direct consequence of gadolinium's very large absorption cross sections is the strong self-shielding of neutrons. This means that thermal neutrons entering a gadolinium-bearing fuel region are very effectively absorbed in its outer layers. As a result, the neutron flux reaching the inner portions of the fuel rod is significantly attenuated compared to the flux at its surface. This effect greatly reduces the effective absorption reaction rate in gadolinium compared to the value that would be calculated assuming a uniform neutron flux throughout the rod volume. Consequently [6]:

- standard diffusion-theory approaches may be insufficient. High-resolution neutron transport methods, such as the Method of Characteristics (MOC) or Monte Carlo techniques, are required to better capture the steep flux gradients in the presence of strong absorbers;
- simple averaging of neutron properties within a computational cell can lead to significant errors if self-shielding effects are not explicitly accounted for. Therefore,

homogenisation of materials in the fuel cell is not applicable here;
- multi-group nuclear data libraries that incorporate self-shielding effects, or dynamic "on-the-fly" generation of effective cross sections during the calculation, must be used.

c) Rapid, non-uniform spatial depletion

The non-uniform spatial depletion of gadolinium—often referred to as the "onion peeling effect"—is a direct consequence of strong self-shielding. Gadolinium does not burn uniformly across the fuel rod volume; instead, the process occurs in layers, starting from the outer regions exposed to the highest neutron flux. These outer layers quickly lose Gd-155 and Gd-157, becoming more "transparent" to neutrons, which then penetrate deeper and deplete the next layer. This creates a depletion front that gradually moves from the rod surface toward its centre.

This highly non-uniform process places significant demands on computational codes:
- to accurately capture steep gadolinium concentration gradients, codes must employ very fine spatial discretisation in regions containing gadolinium. In practice, this means dividing the fuel rod into a series of concentric rings (cylindrical zones), with depletion tracked separately for each [7];
- models treating the entire gadolinium-bearing rod as a homogeneous zone can produce substantial errors, e.g. overestimating absorber depletion rates early in the cycle. This in turn can lead to deviations in calculated reactivity, with the model predicting the reactivity peak too early while a portion of the absorber remains unburned inside the rod.
- the combination of advanced transportation methods, fine spatial meshing, and small time (depletion) steps results in very long simulation times.

d) Sensitivity to irradiation history and lack of validation data

The depletion rate of gadolinium is sensitive not only to fuel design but also to the detailed irradiation history and local reactor operating parameters, such as fuel temperature, moderator density (steam fraction in BWRs), or the presence of control rods [8]. The complex, coupled effects of these parameters further complicate analysis.

However, the greatest limitation in improving simulation tools is the insufficient amount of high-quality experimental data. This is particularly true for the isotopic composition of burned BWR gadolinium-bearing fuel, especially at low depletion levels where the reactivity peak occurs [9]. Existing datasets often lack precise measurements of residual gadolinium isotope concentrations. This means that even if computational codes are theoretically capable of modelling complex phenomena, confidence in the accuracy of their predictions is limited by the shortage of data for comparison and validation.

4. Consequences of the reactivity peak and requirements for safety analyses

The presence of gadolinium in nuclear fuel leads to a characteristic non-monotonic behaviour of reactivity as a function of depletion. In contrast to fuel without burnable absorbers—where reactivity generally decreases—an initial increase is observed here. This occurs because the transmutation rate of the Gd-155 and Gd-157 isotopes is initially much faster than the depletion rate of the fissionable material. At the point where most of the effective gadolinium isotopes have been depleted, the reactivity curve reaches a maximum, referred to as the „reactivity peak". After this point, the dominant effects become the loss of fissionable material and the continued buildup of fission products, resulting in a systematic decrease in reactivity.

Although the reactivity peak occurs only during reactor operation, it has fundamental importance for subsequent criticality safety analyses—for example, for spent fuel pools or transport flasks [10]. Such analyses must be based on conservative assumptions regarding the fuel state. Since a storage facility may contain assemblies at different depletion levels, it is necessary to identify the most reactive isotopic composition the fuel could have reached at any point in its operational history. For gadolinium-bearing nuclear fuel, this most reactive state does not occur at the beginning of the cycle (when gadolinium suppresses reactivity) or at the end of the cycle (when the fuel is heavily depleted). Instead, it occurs precisely at the moment the reactivity peak is reached. For this reason, accurately predicting the isotopic composition of the fuel at this specific point is a prerequisite for the safe and reliable implementation of the so-called burnup credit concept—an approach in criticality safety analysis that takes into account the reduction in reactivity of spent nuclear fuel due to changes in its composition after reactor operation. An incorrect calculation of nuclide composition at the peak—for example, underestimating the remaining fissile content or overestimating the concentration of poisons—would lead to an inaccurate (non-conservative) assessment of the neutron multiplication factor for storage and transport systems [9].

In summary, although the reactivity peak is a reactor operational phenomenon, it defines the most limiting case for spent fuel safety analyses. The challenge lies not in modelling the peak itself as a process, but in precisely calculating the fuel's isotopic composition at this one critical point in its history. The reliability of such calculations depends directly on the quality of the simulation codes and the nuclear data used [11]. Therefore, international benchmarks, such as the one discussed in this work, play a key role in the verification and validation of computational tools necessary to meet this challenge.

The descriptions of specifications, tables, and figures in this chapter come from the OECD/NEA report [1].

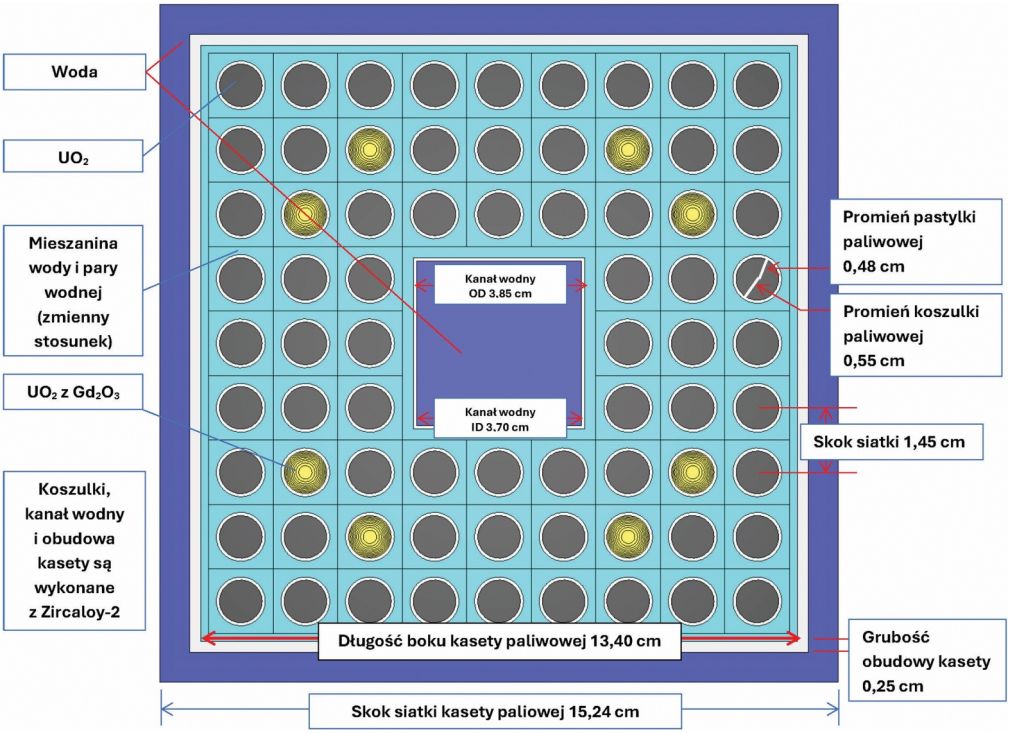

Fig. 2. 2D diagram of the fuel assembly used in the benchmark.

5. Benchmark specification

A) Geometry

Geometrically, the configuration consists of a single 9 9 fuel assembly with reflective boundary conditions. The lattice pitch is uniform across the assembly at 1.45 cm. At the centre of the assembly there is a square water channel containing non-boiling water. Both the water channel and the fuel rod channels are modelled as square regions of identical height. The geometry of the assembly and the fuel rod is shown in Fig. 2.

The primary objective of the benchmark is to further investigate differences in the predicted nuclear densities of gadolinium in spent BWR fuel and their impact on criticality. The benchmark imposes a specific method for modelling gadolinium in order to minimise result discrepancies arising from differences in modelling approaches among participants. Each gadolinium-bearing rod is modelled using 10 concentric rings of equal cross-sectional area, as shown in Fig. 3. Each of the 10 regions in the gadolinium-bearing rod is to be treated separately during depletion calculations, following the numbering shown in Fig. 3 and Table 1. The rings are numbered 1 through 10 from the centre outward. The fuel assembly under consideration contains eight gadolinium-bearing rods located in the positions shown in Fig. 2.

B) Materials

For simplicity, it is assumed that all fuel rods without gadolinium have the same enrichment of 4.0 wt% U-235. All gadolinium-bearing rods are arranged symmetrically and have identical composition. The nuclear densities for fresh fuel and the absorber composition are given in Table 2. The fuel temperature is 900 K. The cladding, water channel, and assembly channel box are made of Zircaloy-2. The temperature of all non-fuel materials is 600 K, consistent with the temperatures used in many continuous-energy cross-section libraries. Three void fraction cases are considered for the water surrounding the fuel rod channels: 0%, 40%, and 70%. The nuclear densities of Zircaloy and water are provided in Table 3.

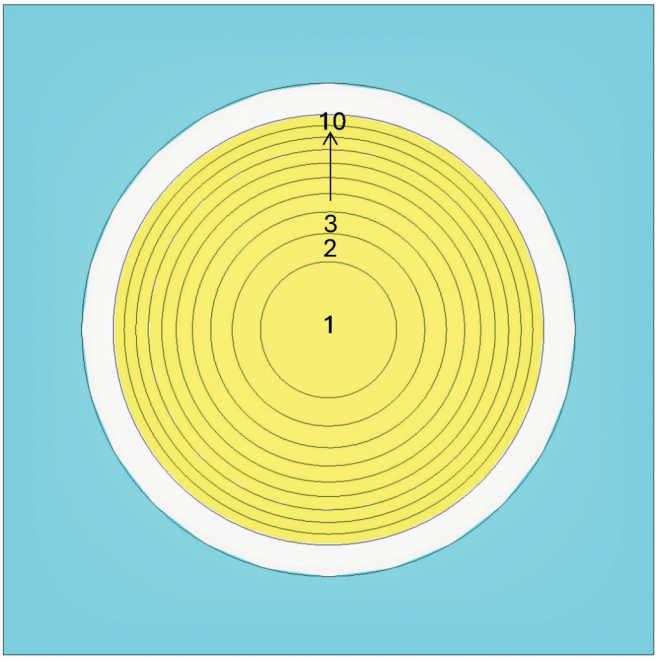

Fig. 3. Details of Gd_2O_3 rod modelling.

C) Depletion conditions

The fuel assembly power is 25.0 MW/MTU (W/gU) throughout the entire depletion period, which is considered as a single continuous operation without shutdowns. The depletion steps are given in Table 4 and were chosen in order to:

1. obtain sufficiently accurate results for most code calculations,
2. provide a precise estimate of reactivity changes in the depletion region where the reactivity maximum occurs.

Participants may add additional steps if deemed necessary to improve accuracy.

The first two steps are 0.1 and 0.4 GWd/MTU, followed by 39 steps of 0.5 GWd/MTU each, yielding a final burnup of 20 GWd/MTU. Depletion calculations are to be performed for the following steam fractions in the water surrounding the fuel rod channels: 0%, 40%, and 70%, using the densities given in Table 3. The water in the central channel and outside the fuel assembly is assumed to contain no steam (0%) in all cases. It is assumed that the temperatures of the fuel, moderator, and structural materials are the same in all three cases.

The assembly design used in the benchmark exhibits several symmetries (half, 1/4 and 1/8), any of which may be applied in the calculations.

D) Required calculation results

The following results were required from all benchmark participants:

a) The infinite multiplication factor (k-inf) for the 2-D configuration for fresh fuel and after each depletion step, without any interim fuel storage period without irradiation.

b) The nuclear number densities of the isotopes listed in Table 5 shall be reported every 2 GWd/MTU:
- without interim storage,
- with a 5-year interim storage period.

c) The average nuclear number densities of actinides and fission products shall be reported for all fuel rods not containing gadolinium. The nuclear number densities of gadolinium isotopes shall be reported for each ring in the gadolinium-bearing rods. The required combinations of depletion and storage time are summarised in Table 6. The depletion of gadolinium-bearing rods shall also be reported for each of the ten steps in Table 6 to assess potential differences in depletion arising from modelling of gadolinium absorption.

An Excel spreadsheet was provided to facilitate the submission of results. Participants were also requested to provide general information, including details relevant for comparing results among participants, namely:

1. Name of the calculation code used,
2. Neutronic/spectral calculation method (e.g., Monte Carlo, S_n, MOC),

Table 1. Dimensions of gadolinium rod rings [1].

Ring number	External radius [cm]
1	0.151789
2	0.214663
3	0.262907
4	0.303579
5	0.339411
6	0.371806
7	0.401597
8	0.429325
9	0.455368
10	0.48

Table 2. Isotopic composition of fuel and absorber [1].

Material	Isotope/Element	Nuclear density [atom/b·cm]
UO_2	U-234	8.4700×10^{-6}
	U-235	9.4763×10^{-4}
	U-238	2.2447×10^{-2}
	O	4.6807×10^{-2}
$UO_2 + Gd_2O_3$	U-234	6.8396×10^{-6}
	U-235	7.6521×10^{-4}
	U-238	2.1460×10^{-2}
	O	4.6225×10^{-2}
	Gd-154	2.5654×10^{-5}
	Gd-155	1.7417×10^{-4}
	Gd-156	2.4089×10^{-4}
	Gd-157	1.8417×10^{-4}
	Gd-158	2.9232×10^{-4}
	Gd-160	2.5725×10^{-4}

Table 3. Isotopic composition of water and Zircaloy [1].

Material	Element	Nuclear density [atoms/b·cm]
Water (0% steam void)	H	4.3417×10^{-2}
	O	2.1708×10^{-2}
Water with 40% steam void	H	2.7998×10^{-2}
	O	1.3999×10^{-2}
Water with 70% steam void	H	1.6434×10^{-2}
	O	8.2170×10^{-3}
Zircaloy-2	Sn	4.9797×10^{-4}
	Fe	9.1782×10^{-5}
	Cr	7.5861×10^{-5}
	Ni	4.0314×10^{-5}
	Zr	4.2465×10^{-2}

3. Depletion calculation method (e.g., predictor–corrector, predictor only, iterative predictor–corrector, midpoint method)
4. Nuclear data library (e.g., ENDF/B-VII.1, JEFF-3.1),
5. Number of energy groups (or continuous-energy neutron flux spectrum),
6. Portion of the assembly modelled (e.g., full assembly, half assembly, etc.)
7. Convergence criterion (e.g., source and flux, or k_{eff} and value),
8. Optional description of the code.

6. Results

Depletion calculations for the analysed BWR fuel assembly were performed using the TRITON calculation sequence from the SCALE code package, version 6.2.2 [12]. The SCALE package, developed by Oak Ridge National Laboratory, is an integrated set of tools for modelling and safety analysis of nuclear systems. Within the TRITON sequence, the two-dimensional deterministic solver NEWT, based on the discrete ordinates method (Sn), was used to solve the neutron transport equation. Coupling between transport calculations and depletion calculations was carried out using the predictor–corrector method.

Table 4. Depletion steps [1].

Step No.	Length[a]	Cumulative depletion ratio[b]	Step No.	Length[a]	Cumulative depletion ratio[b]
1	0.10	0.10	32	0.25	7.75
2	0.15	0.25	33	0.25	8.00
3	0.25	0.50	34	0.25	8.25
4	0.25	0.75	35	0.25	8.50
5	0.25	1.00	36	0.25	8.75
6	0.25	1.25	37	0.25	9.00
7	0.25	1.50	38	0.25	9.25
8	0.25	1.75	39	0.25	9.50
9	0.25	2.00	40	0.25	9.75
10	0.25	2.25	41	0.25	10.0
11	0.25	2.50	42	0.5	10.5
12	0.25	2.75	43	0.5	11.0
13	0.25	3.00	44	0.5	11.5
14	0.25	3.25	45	0.5	12.0
15	0.25	3.50	46	0.5	12.5
16	0.25	3.75	47	0.5	13.0
17	0.25	4.00	48	0.5	13.5
18	0.25	4.25	49	0.5	14.0
19	0.25	4.50	50	0.5	14.5
20	0.25	4.75	51	0.5	15.0
21	0.25	5.00	52	0.5	15.5
22	0.25	5.25	53	0.5	16.0
23	0.25	5.50	54	0.5	16.5
24	0.25	5.75	55	0.5	17.0
25	0.25	6.00	56	0.5	17.5
26	0.25	6.25	57	0.5	18.0
27	0.25	6.50	58	0.5	18.5
28	0.25	6.75	59	0.5	19.0
29	0.25	7.00	60	0.5	19.5
30	0.25	7.25	61	0.5	20.0
31	0.25	7.50			

[a] Depletion step length is given in GWd/MTU.
[b] The cumulative depletion ratio is given in GWd/MTU.

Table 5. Isotopes to report [1].

Actinides	U-234, 235, 236, 238, Np-237, Pu-238, 239, 240, 241, 242, Am-241
Fission products	Tc-99, Rh-103, Xe-131, Eu-155, Cs-133, Nd-143, 148, Sm-147, 149, 151, 152
Gd	Gd-154, 155, 156, 157, 158, 160

Table 6. Burnup and decay times for reporting [1].

Burnup ratio [GWd/MTU]	Storage period [years]
2	0 and 5
4	0 and 5
6	0 and 5
8	0 and 5
10	0 and 5
12	0 and 5
14	0 and 5
16	0 and 5
18	0 and 5
20	0 and 5

The computational model was developed in accordance with the benchmark specification [1]. A full 9 9 fuel assembly configuration was modelled without applying symmetry simplifications, which was one of the modelling options adopted by benchmark participants. In accordance with the benchmark assumptions, reflective boundary conditions were applied at the external boundaries of the assembly for the calculation of the infinite multiplication factor (k-inf), thereby simulating an infinite lattice of identical assemblies. A key element of the specification was the detailed modelling of gadolinium-bearing fuel rods, which were divided into ten concentric zones of equal cross-sectional area to enable accurate tracking of poison depletion. Calculations were performed using the 252-group neutron data library based on ENDF/B-VII.1, supplied with the SCALE package.

This paper presents selected results relevant to the requirements of the benchmark authors. Figure 4 shows the variation of the multiplication factor k-inf as a function of burnup for three analysed steam fractions. Tables 7 and 8 summarise the calculated nuclear number densities for the most important actinides and fission products from the standpoint of criticality, taking into account different burnup ratio, steam fractions, and a 5-year cooling period. The key benchmark aspect of gadolinium poison depletion is illustrated in Figures 5 and 6, where, for isotopes Gd-155 and Gd-157, the changes in their total number density (summed over all rings) are shown as a function of depletion and steam fraction. Figure 7 presents the relationship between the depletion of gadolinium-bearing rods and the depletion of the entire fuel assembly. Due to data rights, the results of other teams were not reproduced here. Aggregate comparisons are available in Annex B of the OECD/NEA report, where SC20 rows in Gd-155/Gd-157 concentration tables (e.g., pp. 117–122 [1]) show the same order of magnitude as other participants; similarly, k-inf results and corresponding burnups are compiled (Tab. 4.2 [1]). The OECD/NEA report [1] noted that 'SC20 actinide results indicate an error in the initial uranium isotopic concentrations' and for this reason, SC20 results were not included in the statistical analyses of actinides. This note applies solely to actinides and selected fission products – it does not refer to the gadolinium comparisons or k-inf trends presented here.

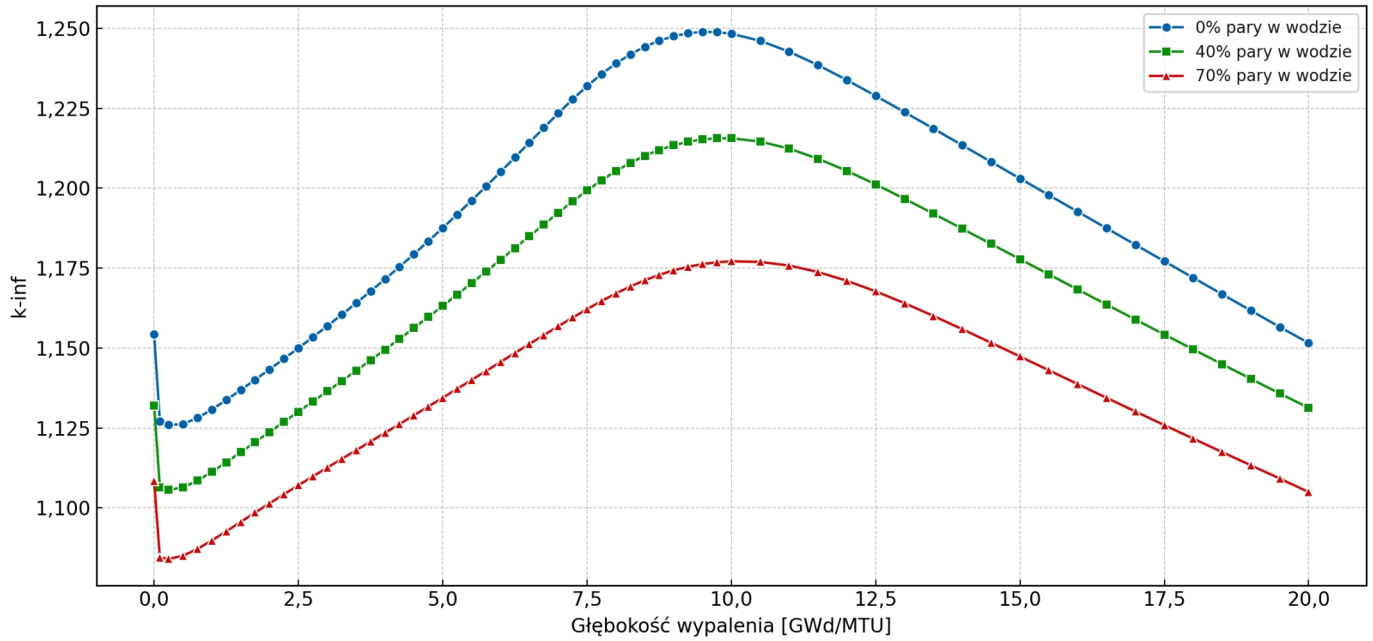

Fig. 4. Changes in the k-inf multiplication factor as a function of burnup for the three analysed water steam void fractions.

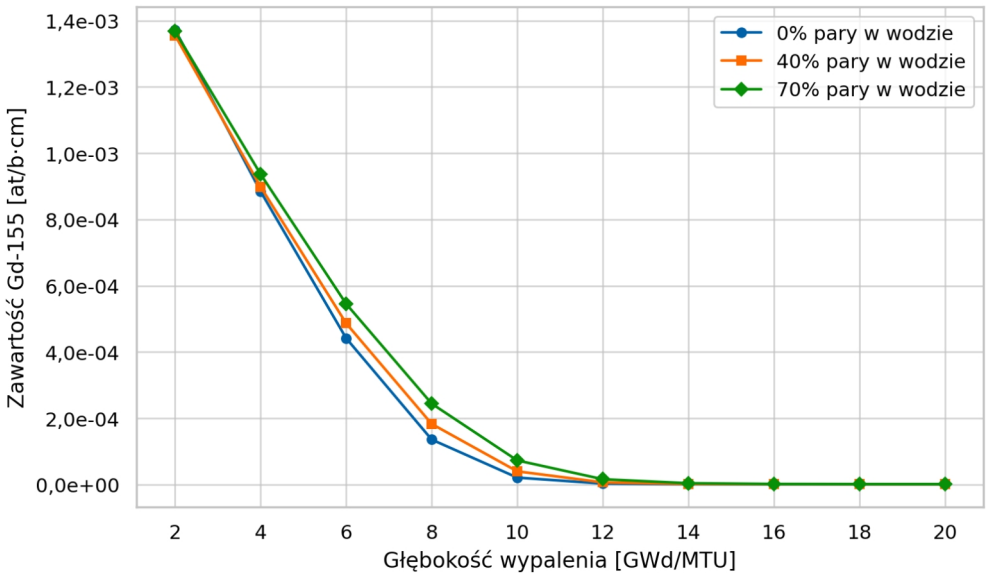

Fig. 5. Changes in the total Gd-155 nuclear density across all rings depending on burnup and steam content.

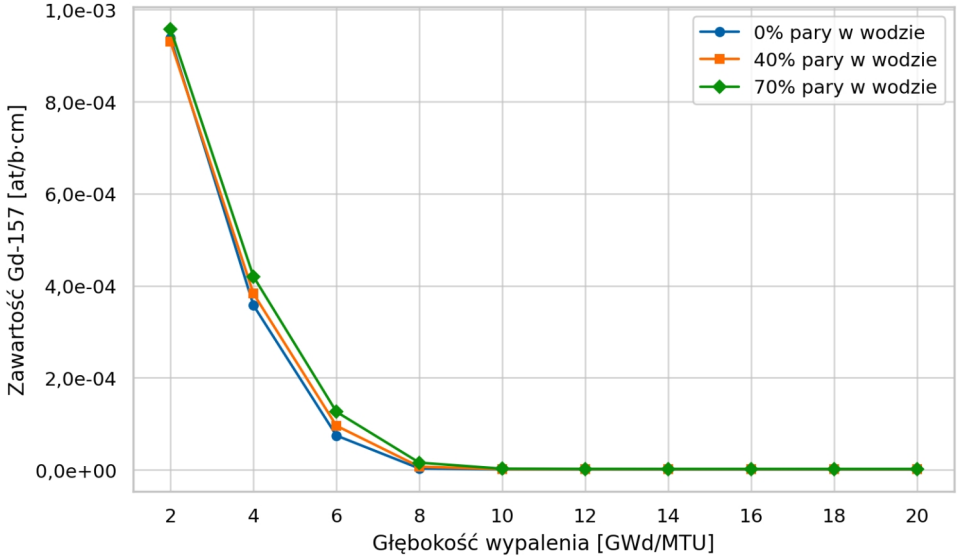

Fig. 6. Changes in the total Gd-157 nuclear density across all rings depending on burnup and steam content.

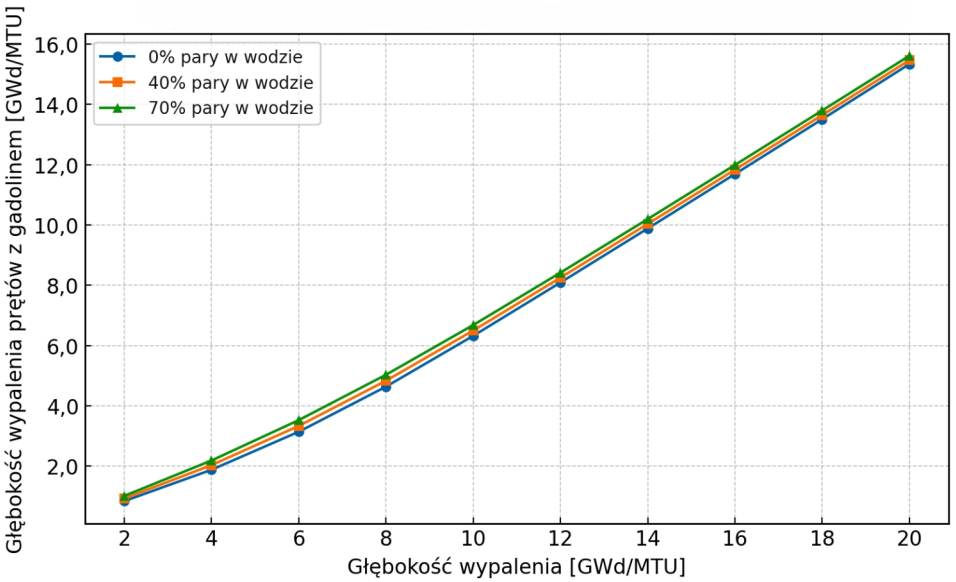

Fig. 7. The relationship between the burnup of gadolinium rods and the burnup of the entire fuel assembly.

Table 7. Calculated nuclear densities for the most important actinides from the point of view of criticality, taking into account different burn-up, steam content and a 5-year cooling time.

Steam void fraction [%	Burnup ratio [GWd/MTU]	Storage time [years]	Nuclear densities of actinides [atom/barn·cm]										
			U-234	U-235	U-236	U-238	Np-237	Pu-238	Pu-239	Pu-240	Pu-241	Pu-242	Am-241
0	2	0	8.0919E–06	8.7188E–04	1.0068E–05	2.2313E–02	1.4632E–07	2.2230E–09	1.8703E–05	6.8719E–07	6.0084E–08	7.8557E-10	1.5664E-10
0	2	5	8.0919E–06	8.7188E–04	1.0069E–05	2.2313E–02	1.7169E–07	2.3455E–09	1.9621E–05	6.8683E–07	4.7152E–08	7.8561E-10	1.3033E–08
0	4	0	7.9014E–06	8.1942E–04	1.9468E–05	2.2289E–02	3.8288E–07	1.2122E–08	3.4412E–05	2.4179E–06	4.0231E–07	1.1063E–08	2.1584E–09
0	4	5	7.9015E–06	8.1943E–04	1.9468E–05	2.2289E–02	4.1901E–07	1.3695E–08	3.5310E–05	2.4175E–06	3.0753E–07	1.0764E–08	9.6877E–08
0	6	0	7.7171E–06	7.6944E–04	2.8298E–05	2.2265E–02	6.7703E–07	3.2176E–08	4.6926E–05	4.7667E–06	1.0986E–06	4.7512E–08	9.0197E–09
0	6	5	7.7180E–06	7.6944E–04	2.8298E–05	2.2265E–02	7.2543E–07	4.3407E–08	4.7803E–05	4.7649E–06	8.0128E–07	4.4986E–08	3.0701E–07
0	8	0	7.5384E–06	7.2151E–04	3.6629E–05	2.2241E–02	1.0141E–06	6.4093E–08	5.6810E–05	7.4960E–06	2.0979E–06	1.2684E–07	2.3319E–08
0	8	5	7.5421E–06	7.2148E–04	3.6633E–05	2.2241E–02	1.0782E–06	1.0504E–07	5.7668E–05	7.4928E–06	1.4559E–06	1.1729E–07	6.7046E–07
0	10	0	7.3640E–06	6.7541E–04	4.4524E–05	2.2217E–02	1.3861E–06	1.0948E–07	6.4645E–05	1.0459E–05	3.3271E–06	2.6282E–07	4.6568E–08
0	10	5	7.3744E–06	6.7531E–04	4.4536E–05	2.2217E–02	1.4718E–06	2.1394E–07	6.5497E–05	1.0456E–05	2.2014E–06	2.3807E–07	1.1900E–06
0	12	0	7.1914E–06	6.3109E–04	5.2024E–05	2.2194E–02	1.7931E–06	1.7056E–07	7.0990E–05	1.3566E–05	4.7355E–06	4.6720E–07	7.9351E–08
0	12	5	7.2147E–06	6.3086E–04	5.2052E–05	2.2193E–02	1.9082E–06	3.8641E–07	7.1852E–05	1.3566E–05	3.0021E–06	4.1578E–07	1.8558E–06
0	14	0	7.0196E–06	5.8851E–04	5.9151E–05	2.2169E–02	2.2349E–06	2.4986E–07	7.6181E–05	1.6763E–05	6.2754E–06	7.5010E–07	1.2158E–07
0	14	5	7.0650E–06	5.8810E–04	5.9202E–05	2.2169E–02	2.3877E–06	6.3824E–07	7.7061E–05	1.6770E–05	3.8319E–06	6.5769E–07	2.6499E–06
0	16	0	6.8484E–06	5.4762E–04	6.5916E–05	2.2144E–02	2.7082E–06	3.4981E–07	8.0401E–05	2.0010E–05	7.8963E–06	1.1196E–06	1.7259E–07
0	16	5	6.9285E–06	5.4695E–04	6.6000E–05	2.2144E–02	2.9074E–06	9.8308E–07	8.1303E–05	2.0031E–05	4.6668E–06	9.6951E–07	3.5488E–06
0	18	0	6.6776E–06	5.0837E–04	7.2328E–05	2.2119E–02	3.2089E–06	4.7272E–07	8.3779E–05	2.3276E–05	9.5543E–06	1.5818E–06	2.3120E–07
0	18	5	6.8091E–06	5.0738E–04	7.2454E–05	2.2118E–02	3.4639E–06	1.4321E–06	8.4709E–05	2.3320E–05	5.4907E–06	1.3557E–06	4.5261E–06
0	20	0	6.5072E–06	4.7074E–04	7.8394E–05	2.2092E–02	3.7334E–06	6.2081E–07	8.6430E–05	2.6536E–05	1.1213E–05	2.1413E–06	2.9591E–07
0	20	5	6.7108E–06	4.6936E–04	7.8571E–05	2.2092E–02	4.0536E–06	1.9937E–06	8.7393E–05	2.6611E–05	6.2945E–06	1.8199E–06	5.5550E–06
40	2	0	8.0696E–06	8.7230E–04	1.0398E–05	2.2309E–02	1.7064E–07	2.8752E–09	2.1276E–05	7.7949E–07	7.9735E–08	1.0286E–09	2.0881E-10
40	2	5	8.0697E–06	8.7231E–04	1.0398E–05	2.2309E–02	2.0051E–07	3.0344E–09	2.2319E–05	7.7909E–07	6.2573E–08	1.0287E–09	1.7297E–08
40	4	0	7.8592E–06	8.2065E–04	2.0028E–05	2.2282E–02	4.4888E–07	1.5723E–08	3.9153E–05	2.6886E–06	5.2000E–07	1.4049E–08	2.8102E–09
40	4	5	7.8594E–06	8.2066E–04	2.0027E–05	2.2282E–02	4.9188E–07	1.7889E–08	4.0172E–05	2.6881E–06	3.9711E–07	1.3686E–08	1.2539E–07
40	6	0	7.6568E–06	7.7174E–04	2.9012E–05	2.2255E–02	7.9499E–07	4.1758E–08	5.3485E–05	5.2301E–06	1.3908E–06	5.8830E–08	1.1521E–08
40	6	5	7.6580E–06	7.7175E–04	2.9011E–05	2.2255E–02	8.5321E–07	5.6885E–08	5.4480E–05	5.2282E–06	1.0120E–06	5.5845E–08	3.8970E–07
40	8	0	7.4617E–06	7.2512E–04	3.7438E–05	2.2227E–02	1.1913E–06	8.3155E–08	6.4943E–05	8.1504E–06	2.6150E–06	1.5378E–07	2.9336E–08
40	8	5	7.4666E–06	7.2509E–04	3.7440E–05	2.2227E–02	1.2691E–06	1.3712E–07	6.5917E–05	8.1476E–06	1.8077E–06	1.4272E–07	8.3802E–07
40	10	0	7.2724E–06	6.8050E–04	4.5376E–05	2.2201E–02	1.6270E–06	1.4181E–07	7.4146E–05	1.1300E–05	4.0946E–06	3.1281E–07	5.7881E–08

40	10	5	7.2859E–06	6.8039E–04	4.5386E–05	2.2201E–02	1.7314E–06	2.7690E–07	7.5112E–05	1.1298E–05	2.6937E–06	2.8462E–07	1.4682E–06
40	12	0	7.0868E–06	6.3776E–04	5.2879E–05	2.2173E–02	2.0998E–06	2.2019E–07	8.1691E–05	1.4585E–05	5.7617E–06	5.4648E–07	9.7641E–08
40	12	5	7.1167E–06	6.3751E–04	5.2905E–05	2.2173E–02	2.2397E–06	4.9452E–07	8.2667E–05	1.4589E–05	3.6234E–06	4.8876E–07	2.2636E–06
40	14	0	6.9034E–06	5.9685E–04	5.9976E–05	2.2146E–02	2.6087E–06	3.2111E–07	8.7978E–05	1.7951E–05	7.5634E–06	8.6308E–07	1.4834E–07
40	14	5	6.9612E–06	5.9639E–04	6.0027E–05	2.2146E–02	2.7941E–06	8.0697E–07	8.8975E–05	1.7965E–05	4.5708E–06	7.6072E–07	3.2002E–06
40	16	0	6.7219E–06	5.5770E–04	6.6685E–05	2.2118E–02	3.1503E–06	4.4728E–07	9.3223E–05	2.1358E–05	9.4477E–06	1.2686E–06	2.0915E–07
40	16	5	6.8231E–06	5.5696E–04	6.6770E–05	2.2118E–02	3.3913E–06	1.2283E–06	9.4248E–05	2.1391E–05	5.5135E–06	1.1044E–06	4.2503E–06
40	18	0	6.5422E–06	5.2025E–04	7.3019E–05	2.2089E–02	3.7198E–06	6.0116E–07	9.7570E–05	2.4778E–05	1.1369E–05	1.7671E–06	2.7876E–07
40	18	5	6.7066E–06	5.1917E–04	7.3147E–05	2.2089E–02	4.0270E–06	1.7691E–06	9.8631E–05	2.4840E–05	6.4361E–06	1.5224E–06	5.3845E–06
40	20	0	6.3644E–06	4.8444E–04	7.8989E–05	2.2060E–02	4.3127E–06	7.8500E–07	1.0114E–04	2.8187E–05	1.3289E–05	2.3606E–06	3.5557E–07
40	20	5	6.6166E–06	4.8295E–04	7.9168E–05	2.2059E–02	4.6967E–06	2.4367E–06	1.0224E–04	2.8288E–05	7.3301E–06	2.0161E–06	6.5742E–06
70	2	0	8.0473E–06	8.7273E–04	1.0746E–05	2.2306E–02	1.9567E–07	3.6415E–09	2.3881E–05	8.6431E–07	1.0168E–07	1.2875E–09	2.6767E-10
70	2	5	8.0473E–06	8.7274E–04	1.0746E–05	2.2306E–02	2.3033E–07	3.8457E–09	2.5048E–05	8.6381E–07	7.9791E–08	1.2875E–09	2.2058E–08
70	4	0	7.8169E–06	8.2186E–04	2.0631E–05	2.2275E–02	5.1674E–07	1.9969E–08	4.4033E–05	2.9250E–06	6.4508E–07	1.7023E–08	3.5145E–09
70	4	5	7.8171E–06	8.2187E–04	2.0630E–05	2.2275E–02	5.6716E–07	2.2831E–08	4.5174E–05	2.9242E–06	4.9205E–07	1.6602E–08	1.5579E–07
70	6	0	7.5963E–06	7.7398E–04	2.9802E–05	2.2244E–02	9.1548E–07	5.3060E–08	6.0366E–05	5.6255E–06	1.6900E–06	6.9436E–08	1.4133E–08
70	6	5	7.5978E–06	7.7399E–04	2.9800E–05	2.2244E–02	9.8446E–07	7.2505E–08	6.1482E–05	5.6233E–06	1.2264E–06	6.6092E–08	4.7485E–07
70	8	0	7.3846E–06	7.2859E–04	3.8360E–05	2.2214E–02	1.3710E–06	1.0561E–07	7.3638E–05	8.7070E–06	3.1310E–06	1.7765E–07	3.5458E–08
70	8	5	7.3907E–06	7.2856E–04	3.8360E–05	2.2213E–02	1.4640E–06	1.7347E–07	7.4733E–05	8.7043E–06	2.1552E–06	1.6554E–07	1.0061E–06
70	10	0	7.1805E–06	6.8536E–04	4.6384E–05	2.2183E–02	1.8696E–06	1.7982E–07	8.4487E–05	1.2023E–05	4.8474E–06	3.5486E–07	6.9177E–08
70	10	5	7.1971E–06	6.8524E–04	4.6390E–05	2.2183E–02	1.9945E–06	3.4662E–07	8.5575E–05	1.2022E–05	3.1699E–06	3.2449E–07	1.7419E–06
70	12	0	6.9818E–06	6.4410E–04	5.3934E–05	2.2153E–02	2.4062E–06	2.7823E–07	9.3522E–05	1.5478E–05	6.7558E–06	6.0977E–07	1.1567E–07
70	12	5	7.0186E–06	6.4383E–04	5.3955E–05	2.2153E–02	2.5730E–06	6.1149E–07	9.4622E–05	1.5485E–05	4.2140E–06	5.4845E–07	2.6587E–06
70	14	0	6.7870E–06	6.0473E–04	6.1048E–05	2.2122E–02	2.9783E–06	4.0384E–07	1.0119E–04	1.9016E–05	8.7986E–06	9.4833E–07	1.7451E–07
70	14	5	6.8576E–06	6.0425E–04	6.1094E–05	2.2122E–02	3.1983E–06	9.8541E–07	1.0231E–04	1.9037E–05	5.2616E–06	8.4087E–07	3.7270E–06
70	16	0	6.5955E–06	5.6718E–04	6.7752E–05	2.2090E–02	3.5825E–06	5.5953E–07	1.0774E–04	2.2596E–05	1.0926E–05	1.3742E–06	2.4470E–07
70	16	5	6.7181E–06	5.6642E–04	6.7831E–05	2.2090E–02	3.8672E–06	1.4821E–06	1.0891E–04	2.2642E–05	6.2947E–06	1.2037E–06	4.9157E–06
70	18	0	6.4072E–06	5.3136E–04	7.4061E–05	2.2059E–02	4.2139E–06	7.4783E–07	1.1336E–04	2.6190E–05	1.3093E–05	1.8891E–06	3.2490E–07
70	18	5	6.6049E–06	5.3025E–04	7.4182E–05	2.2058E–02	4.5748E–06	2.1114E–06	1.1457E–04	2.6272E–05	7.3004E–06	1.6375E–06	6.1939E–06
70	20	0	6.2221E–06	4.9721E–04	7.9990E–05	2.2026E–02	4.8674E–06	9.7094E–07	1.1814E–04	2.9776E–05	1.5264E–05	2.4933E–06	4.1347E–07
70	20	5	6.5230E–06	4.9568E–04	8.0162E–05	2.2025E–02	5.3160E–06	2.8790E–06	1.1942E–04	2.9907E–05	8.2716E–06	2.1419E–06	7.5324E–06

Table 8. Calculated nuclear densities for the most important fission products from the point of view of criticality, taking into account different burn-up, steam content and a 5-year cooling time.

Steam void fraction [%]	Burnup ratio [GWd/MTU]	Storage time [years]	Nuclear densities of fission products [atom/barn·cm]										
			Tc-99	Rh-103	Xe-131	Cs-133	Nd-143	Nd-148	Sm-147	Sm-149	Sm-151	Sm-152	Eu-155
0	2	0	2.8460E–06	7.3955E–07	1.2166E–06	2.9378E–06	2.1011E–06	8.4670E–07	2.0953E–08	7.9082E–08	1.5038E–07	2.0197E–07	1.3566E–08
0	2	5	3.0077E–06	1.6208E–06	1.4374E–06	3.3096E–06	2.8635E–06	8.4673E–07	7.9810E–07	1.0224E–07	1.4934E–07	2.0200E–07	6.5494E–09
0	4	0	5.8255E–06	2.1418E–06	2.6265E–06	6.2104E–06	4.8391E–06	1.6931E–06	9.5949E–08	8.2212E–08	2.2802E–07	4.7831E–07	2.1982E–08
0	4	5	5.9871E–06	3.2678E–06	2.8499E–06	6.5830E–06	5.6011E–06	1.6910E–06	1.7697E–06	1.0368E–07	2.2164E–07	4.7583E–07	9.2503E–09
0	6	0	8.7798E–06	3.7180E–06	4.0116E–06	9.4491E–06	7.4729E–06	2.5379E–06	2.1926E–07	7.9684E–08	2.6982E–07	7.8193E–07	2.9207E–08
0	6	5	8.9410E–06	4.9253E–06	4.2369E–06	9.8227E–06	8.2241E–06	2.5337E–06	2.7589E–06	9.9179E–08	2.5943E–07	7.7477E–07	1.1423E–08
0	8	0	1.1711E–05	5.3406E–06	5.3714E–06	1.2656E–05	9.9972E–06	3.3817E–06	3.8398E–07	7.7184E–08	2.9296E–07	1.0940E–06	3.6831E–08
0	8	5	1.1872E–05	6.5828E–06	5.5983E–06	1.3031E–05	1.0739E–05	3.3753E–06	3.7312E–06	9.5049E–08	2.7971E–07	1.0806E–06	1.3671E–08
0	10	0	1.4620E–05	6.9706E–06	6.7040E–06	1.5830E–05	1.2414E–05	4.2246E–06	5.8411E–07	7.6224E–08	3.0555E–07	1.4055E–06	4.5417E–08
0	10	5	1.4779E–05	8.2311E–06	6.9319E–06	1.6205E–05	1.3147E–05	4.2159E–06	4.6784E–06	9.2682E–08	2.9022E–07	1.3845E–06	1.6084E–08
0	12	0	1.7499E–05	8.5907E–06	8.0046E–06	1.8965E–05	1.4720E–05	5.0660E–06	8.1398E–07	7.5660E–08	3.1337E–07	1.7092E–06	5.5170E–08
0	12	5	1.7657E–05	9.8616E–06	8.2330E–06	1.9339E–05	1.5443E–05	5.0549E–06	5.5962E–06	9.0805E–08	2.9627E–07	1.6797E–06	1.8712E–08
0	14	0	2.0347E–05	1.0192E–05	9.2699E–06	2.2055E–05	1.6912E–05	5.9058E–06	1.0682E–06	7.4990E–08	3.1930E–07	2.0015E–06	6.6316E–08
0	14	5	2.0502E–05	1.1468E–05	9.4982E–06	2.2429E–05	1.7625E–05	5.8920E–06	6.4820E–06	8.8949E–08	3.0045E–07	1.9624E–06	2.1635E–08
0	16	0	2.3162E–05	1.1768E–05	1.0498E–05	2.5100E–05	1.8988E–05	6.7439E–06	1.3420E–06	7.4098E–08	3.2414E–07	2.2819E–06	7.9036E–08
0	16	5	2.3314E–05	1.3045E–05	1.0726E–05	2.5471E–05	1.9689E–05	6.7272E–06	7.3350E–06	8.7028E–08	3.0341E–07	2.2321E–06	2.4908E–08
0	18	0	2.5943E–05	1.3317E–05	1.1688E–05	2.8097E–05	2.0947E–05	7.5804E–06	1.6308E–06	7.3000E–08	3.2817E–07	2.5506E–06	9.3399E–08
0	18	5	2.6090E–05	1.4590E–05	1.1914E–05	2.8465E–05	2.1634E–05	7.5605E–06	8.1545E–06	8.5055E–08	3.0542E–07	2.4887E–06	2.8556E–08
0	20	0	2.8689E–05	1.4834E–05	1.2839E–05	3.1045E–05	2.2786E–05	8.4155E–06	1.9307E–06	7.1731E–08	3.3153E–07	2.8079E–06	1.0939E–07
0	20	5	2.8830E–05	1.6099E–05	1.3062E–05	3.1408E–05	2.3457E–05	8.3919E–06	8.9400E–06	8.3049E–08	3.0664E–07	2.7322E–06	3.2594E–08
40	2	0	2.8391E–06	7.4610E–07	1.2151E–06	2.9307E–06	2.0914E–06	8.4721E–07	2.0850E–08	8.6716E–08	1.5491E–07	1.9947E–07	1.3649E–08
40	2	5	3.0005E–06	1.6384E–06	1.4362E–06	3.3019E–06	2.8494E–06	8.4724E–07	7.9478E–07	1.1001E–07	1.5375E–07	1.9950E–07	6.5894E–09
40	4	0	5.8070E–06	2.1625E–06	2.6192E–06	6.1901E–06	4.8149E–06	1.6937E–06	9.5048E–08	9.1415E–08	2.3970E–07	4.6909E–07	2.2002E–08
40	4	5	5.9682E–06	3.3055E–06	2.8432E–06	6.5621E–06	5.5715E–06	1.6915E–06	1.7565E–06	1.1263E–07	2.3273E–07	4.6670E–07	9.3423E–09
40	6	0	8.7455E–06	3.7555E–06	3.9943E–06	9.4101E–06	7.4346E–06	2.5381E–06	2.1628E–07	8.9372E–08	2.8839E–07	7.6386E–07	2.9330E–08
40	6	5	8.9062E–06	4.9829E–06	4.2203E–06	9.7829E–06	8.1796E–06	2.5338E–06	2.7303E–06	1.0817E–07	2.7675E–07	7.5688E–07	1.1634E–08
40	8	0	1.1657E–05	5.3949E–06	5.3398E–06	1.2593E–05	9.9464E–06	3.3810E–06	3.7725E–07	8.6747E–08	3.1756E–07	1.0654E–06	3.7251E–08
40	8	5	1.1817E–05	6.6587E–06	5.5673E–06	1.2966E–05	1.0682E–05	3.3745E–06	3.6824E–06	1.0358E–07	3.0232E–07	1.0521E–06	1.4040E–08
40	10	0	1.4542E–05	7.0410E–06	6.6545E–06	1.5737E–05	1.2355E–05	4.2228E–06	5.7170E–07	8.5891E–08	3.3518E–07	1.3649E–06	4.6330E–08

40	10	5	1.4700E–05	8.3235E–06	6.8830E–06	1.6111E–05	1.3081E–05	4.2139E–06	4.6055E–06	1.0106E–07	3.1712E–07	1.3440E–06	1.6643E–08
40	12	0	1.7396E–05	8.6761E–06	7.9346E–06	1.8839E–05	1.4658E–05	5.0629E–06	7.9387E–07	8.5719E–08	3.4699E–07	1.6556E–06	5.6739E–08
40	12	5	1.7552E–05	9.9688E–06	8.1635E–06	1.9212E–05	1.5375E–05	5.0516E–06	5.4960E–06	9.9358E–08	3.2649E–07	1.6259E–06	1.9472E–08
40	14	0	2.0217E–05	1.0291E–05	9.1769E–06	2.1893E–05	1.6856E–05	5.9013E–06	1.0384E–06	8.5571E–08	3.5644E–07	1.9334E–06	6.8636E–08
40	14	5	2.0369E–05	1.1588E–05	9.4055E–06	2.2265E–05	1.7562E–05	5.8873E–06	6.3517E–06	9.7802E–08	3.3355E–07	1.8938E–06	2.2588E–08
40	16	0	2.3002E–05	1.1880E–05	1.0380E–05	2.4898E–05	1.8948E–05	6.7379E–06	1.3003E–06	8.5200E–08	3.6466E–07	2.1976E–06	8.2172E–08
40	16	5	2.3150E–05	1.3177E–05	1.0607E–05	2.5267E–05	1.9642E–05	6.7209E–06	7.1716E–06	9.6188E–08	3.3928E–07	2.1469E–06	2.6041E–08
40	18	0	2.5751E–05	1.3440E–05	1.1543E–05	2.7852E–05	2.0933E–05	7.5728E–06	1.5753E–06	8.4586E–08	3.7199E–07	2.4487E–06	9.7403E–08
40	18	5	2.5893E–05	1.4732E–05	1.1768E–05	2.8216E–05	2.1614E–05	7.5524E–06	7.9555E–06	9.4505E–08	3.4396E–07	2.3853E–06	2.9849E–08
40	20	0	2.8464E–05	1.4967E–05	1.2665E–05	3.0754E–05	2.2811E–05	8.4060E–06	1.8596E–06	8.3766E–08	3.7855E–07	2.6872E–06	1.1429E–07
40	20	5	2.8599E–05	1.6250E–05	1.2887E–05	3.1112E–05	2.3476E–05	8.3819E–06	8.7032E–06	9.2772E–08	3.4774E–07	2.6095E–06	3.4013E–08
70	2	0	2.8319E–06	7.5287E–07	1.2133E–06	2.9234E–06	2.0813E–06	8.4785E–07	2.0744E–08	9.5842E–08	1.5964E–07	1.9677E–07	1.3742E–08
70	2	5	2.9931E–06	1.6564E–06	1.4349E–06	3.2941E–06	2.8349E–06	8.4789E–07	7.9152E–07	1.1927E–07	1.5836E–07	1.9680E–07	6.6349E–09
70	4	0	5.7880E–06	2.1828E–06	2.6109E–06	6.1693E–06	4.7900E–06	1.6945E–06	9.4138E–08	1.0267E–07	2.5206E–07	4.5881E–07	2.2035E–08
70	4	5	5.9488E–06	3.3424E–06	2.8354E–06	6.5406E–06	5.5411E–06	1.6923E–06	1.7432E–06	1.2356E–07	2.4446E–07	4.5653E–07	9.4332E–09
70	6	0	8.7104E–06	3.7905E–06	3.9745E–06	9.3698E–06	7.3953E–06	2.5386E–06	2.1329E–07	1.0150E–07	3.0844E–07	7.4335E–07	2.9469E–08
70	6	5	8.8706E–06	5.0368E–06	4.2011E–06	9.7417E–06	8.1342E–06	2.5342E–06	2.7011E–06	1.1946E–07	2.9544E–07	7.3660E–07	1.1835E–08
70	8	0	1.1602E–05	5.4433E–06	5.3042E–06	1.2527E–05	9.8947E–06	3.3808E–06	3.7049E–07	9.8819E–08	3.4470E–07	1.0326E–06	3.7687E–08
70	8	5	1.1761E–05	6.7270E–06	5.5323E–06	1.2899E–05	1.0623E–05	3.3742E–06	3.6322E–06	1.1440E–07	3.2724E–07	1.0196E–06	1.4394E–08
70	10	0	1.4463E–05	7.1009E–06	6.5995E–06	1.5641E–05	1.2294E–05	4.2214E–06	5.5927E–07	9.7909E–08	3.6855E–07	1.3183E–06	4.7265E–08
70	10	5	1.4620E–05	8.4036E–06	6.8285E–06	1.6013E–05	1.3013E–05	4.2125E–06	4.5300E–06	1.1155E–07	3.4739E–07	1.2977E–06	1.7187E–08
70	12	0	1.7292E–05	8.7462E–06	7.8578E–06	1.8708E–05	1.4595E–05	5.0603E–06	7.7378E–07	9.8086E–08	3.8545E–07	1.5946E–06	5.8345E–08
70	12	5	1.7446E–05	1.0059E–05	8.0871E–06	1.9080E–05	1.5304E–05	5.0489E–06	5.3919E–06	1.0995E–07	3.6101E–07	1.5650E–06	2.0220E–08
70	14	0	2.0085E–05	1.0369E–05	9.0763E–06	2.1725E–05	1.6797E–05	5.8973E–06	1.0086E–06	9.8503E–08	3.9923E–07	1.8572E–06	7.1018E–08
70	14	5	2.0235E–05	1.1686E–05	9.3051E–06	2.2095E–05	1.7496E–05	5.8831E–06	6.2160E–06	1.0873E–07	3.7163E–07	1.8174E–06	2.3533E–08
70	16	0	2.2841E–05	1.1965E–05	1.0254E–05	2.4689E–05	1.8902E–05	6.7324E–06	1.2590E–06	9.8776E–08	4.1156E–07	2.1050E–06	8.5381E–08
70	16	5	2.2985E–05	1.3281E–05	1.0481E–05	2.5055E–05	1.9590E–05	6.7151E–06	7.0015E–06	1.0752E–07	3.8071E–07	2.0536E–06	2.7162E–08
70	18	0	2.5559E–05	1.3530E–05	1.1390E–05	2.7600E–05	2.0910E–05	7.5656E–06	1.5206E–06	9.8799E–08	4.2292E–07	2.3385E–06	1.0147E–07
70	18	5	2.5696E–05	1.4840E–05	1.1614E–05	2.7960E–05	2.1585E–05	7.5449E–06	7.7483E–06	1.0624E–07	3.8868E–07	2.2740E–06	3.1121E–08
70	20	0	2.8240E–05	1.5062E–05	1.2484E–05	3.0456E–05	2.2823E–05	8.3970E–06	1.7897E–06	9.8584E–08	4.3349E–07	2.5585E–06	1.1922E–07
70	20	5	2.8368E–05	1.6363E–05	1.2704E–05	3.0808E–05	2.3482E–05	8.3724E–06	8.4567E–06	1.0490E–07	3.9572E–07	2.4795E–06	3.5401E–08

Summary

This paper presents the results obtained by the author within the framework of the OECD/NEA Phase IIB international benchmark on modelling the depletion of BWR-type fuel with gadolinium-bearing rods. The calculations were performed using the SCALE/TRITON 6.2.2 code, applying the discrete ordinates (Sn) method to solve the neutron transport equation, and employing the detailed gadolinium rod model prescribed by the benchmark specification. The presented results clearly reflect the complex physics of the process. The k-inf multiplication factor curves (Fig. 4) correctly illustrate the characteristic reactivity peak, the magnitude of which decreases and whose position shifts towards higher burnup as the steam fraction increases. Analysis of the nuclear number densities of the key gadolinium isotopes Gd-155 and Gd-157 (Figs. 5 and 6) shows a rapid decline, which is the main cause of the initial reactivity rise. As expected, this process occurs fastest for the 0% steam case, where the thermal neutron flux is highest. The relationship between the burnup of gadolinium-bearing rods and the burnup of the entire assembly (Fig. 7) indicates a slower depletion rate of the poison compared to the assembly average, resulting from local neutron flux suppression. Detailed isotopic composition data for actinides and fission products (Tables 7 and 8) provide a complete dataset for further, in-depth safety analyses, e.g. in the framework of the burnup credit concept.

Comparison with the aggregate results published in the OECD/NEA report indicates that the shape of the k-inf curves and the order of magnitude of Gd-155/Gd-157 concentrations for the SC20 submission are consistent with the trends and scatter range presented in the publication. The reactivity peak values for the analyzed steam void fraction variants (approx. 1.250 for 0% void, 1.216 for 40% void, and 1.177 for 70% void) fall within the reported range. At the same time, in accordance with the editorial note of the OECD/NEA report, the SC20 results for actinides indicate a probable error in the initial isotopic composition of uranium, due to which they were not included in the statistical analyses of actinides. For this reason, comparative conclusions for detailed actinide concentrations are not formulated in this text. The presented tables are treated as supplementary material for further analysis.

The general conclusions from the Phase IIB benchmark, as formulated in the OECD report [1], highlight several key aspects. First, the largest source of discrepancies between participants' results proved to be the nuclear data libraries used, with a lesser impact from the calculation code itself or the neutron transport solution method. It was observed that excluding results based on older generations of libraries (e.g., ENDF/B-V) significantly reduced the overall scatter of k-inf values. The benchmark also showed that while concentrations of major isotopes such as U-238 are calculated with very high consistency (deviation below 0.07%), there remain significant uncertainties in predicting the nuclear number densities of key gadolinium isotopes (2sssó up to 44% for Gd-155) and certain fission products, particularly Sm-149, Sm-151, and Eu-155 (2ssssó in the range of 10–26%). These findings underline the importance of continued work on improving nuclear data and validating computational codes, which are essential for reliable spent nuclear fuel safety analyses.

Author's note

M.Sc. Łukasz Koszuk – nuclear physicist, graduate of the Faculty of Physics at the University of Warsaw, currently employed at the Faculty of Physics, Warsaw University of Technology. Co-founder and president of the Forum Atomowe Foundation, he also runs his own consultancy company "AI and Nuclear" and serves as a delegate to the NEA/OECD *Working Party on Nuclear Criticality Safety*.

Bibliography

1. NEA (2022), Burnup Credit Criticality Benchmark Phase IIID: Burnup Calculations of Gadolinium- Bearing Fuel Rods in Boiling Water Reactor Assemblies for Storage and Transportation, OECD Publishing, Paris.
2. Galahom, A. A., et al. (2016). Investigation of different burnable absorbers effects on the neutronic characteristics of PWR assembly. *Journal of Taibah University for Science*, 10(6), 872–882.
3. Rauscher, T., et al. (2019). Cross section measurements of 155,157Gd(n,) induced by thermal and epithermal neutrons. *The European Physical Journal A*, 55(1), 9.
4. Bolukbasi, M., et al. (2017). Performance and economic assessment of enriched gadolinia burnable absorbers. *Nuclear Engineering and Design*, 313, 329–336.
5. Kim, H., et al. (2022). Development of a high performance burnable absorber for soluble-boron-free SMR. *Nuclear Engineering and Technology*, 54(7), 2545–2555.
6. NIST, Atomic Weights and Isotopic Compositions – Gadolinium (Gd), [online].
7. Noguere, G., Leconte, P., Bernard, D., Pottier, M., Paradela, C., Kopecky, S., & Schillebeeckx, P. (2024). Generation of particle self-shielded neutron cross-sections for the Monte-Carlo code TRIPOLI-4®. *EPJ Nuclear Sciences and Technologies*, *10*, Article 18.
8. Radaideh, M. I., et al. (2019). Advanced BWR criticality safety part II: Cask criticality burnup credit sensitivity and uncertainty analyses. Annals of Nuclear Energy, 132, 506–520.
9. Ahn, V. V., et al. (2018). Compound effects of operating parameters on burnup credit in boiling water reactor spent fuel assemblies. Journal of the Korean Physical Society, 72(10), 1229–1238.
10. Clarity, J. B., & Twardowski, T. (2016). An Overview of NRC's BWR Burnup Credit Research Project. PATRAM 2016.
11. Ghrayeb, S., & Wilson, V. (2016). Regulatory research on use of burnup credit for criticality safety in BWR spent fuel transportation packages. In *Proceedings of the 18th International Symposium on the Packaging and Transportation of Radioactive Materials (PATRAM 2016)* (Paper No. 2023). U.S. Nuclear Regulatory Commission.
12. International Atomic Energy Agency. (2007). Implementation of Burnup Credit in Spent Fuel Management Systems. IAEA-TECDOC-1547. Vienna: IAEA.
13. Rearden, Bradley T., & Jessee, Matthew Anderson (2017). SCALE Code System 6.2.2.